

# Odor Communication with Green Leaf Volatiles for Stress Signalling in the Internet of Plants

Fatih Merdan, Ozgur B. Akan, Fellow, IEEE

**Abstract**—This paper develops an end-to-end odor communication model for stress signaling between plants using Green Leaf Volatiles (GLV). A damaged transmitter plant emits (Z)-3-hexenal, (Z)-3-hexenol, and (Z)-3-hexenyl acetate, which propagate through a time-varying diffusion–advection channel and undergo multiplicative loss at the receiver. The sink plant is modeled with a biochemical receiver network that converts the received GLVs into the defensive metabolite (Z)-3-hexenyl  $\beta$ -vicianoside, and an alarm decision is defined based on its concentration level. Numerical results show that (Z)-3-hexenol is the primary driver of the system and that plant perception generally operates in a non-linear region. These findings provide a framework for understanding the evolution of plant-plant communication and for developing next-generation precision farming technologies.

**Index Terms**—Molecular communication, mathematical models, biological processes, plant communication, volatile organic compounds.

## I. Introduction

**P**LANTS are dynamic organisms that actively interact with their environment through a set of chemical signals [1]. To survive various stresses, such as herbivore attacks or extreme temperatures, plants have evolved the ability to release Volatile Organic Compounds (VOCs) [2]. Among these, Green Leaf Volatiles (GLVs) play a critical role in the rapid stress response. When a plant is physically damaged, these molecules are synthesized and released, serving as an airborne “alarm” that neighboring unstressed plants can sense to trigger preemptive defense mechanisms [3], [4]. Characterization of these biological processes through the lens of Information and Communication Technology has emerged as a promising frontier [5]. This interdisciplinary approach allows for the quantification of information flow within ecosystems and provides a framework for designing bio-compatible communication systems [6]. From a communication-theoretic perspective, this interplant interaction can be modeled as a specialized Odor Communication framework [7]. In this framework, the stressed plant acts as a transmitter. The atmosphere serves as a time-varying physical channel where signal propagation is governed by the laws of advection and diffusion. Finally, the neighboring unstressed plant functions as a biological receiver that must decode

these airborne chemical cues through complex internal metabolic pathways to mount an appropriate physiological response.

Early foundational work in this area established an end-to-end model for long-range pheromone communication between plants, characterizing the dispersion of molecules under the laws of turbulent diffusion [8]. More recently, [9] explored the context of stress communication, using continuous gene regulation to approximate Biological Volatile Organic Compound (BVOC) emissions and investigate modulation techniques. Furthermore, [10] evaluates end-to-end behavior via attenuation and delay, emphasizing low-pass characteristics and distance/wind sensitivity. Despite these significant advancements, existing frameworks often simplify the receiver side of the link, frequently treating the sink plant as a basic detector or a generic absorption point. Furthermore, many models rely on static or simplified channel assumptions that do not fully capture airborne particle communication. In this paper, three primary contributions are presented. First, a rigorous biochemical receiver model is developed that is rooted in recent biological experimental data. Specifically, the internal metabolic transformation of Green Leaf Volatiles comprising (Z)-3-hexenal, (Z)-3-hexenol, and (Z)-3-hexenyl acetate into the defensive glycoside (Z)-3-hexenyl  $\beta$ -vicianoside is characterized. Through modeling of these metabolic pathways, (Z)-3-hexenol is identified as the main driver of the defensive state, providing a biological basis for signal reception. Second, a completely characterized time-varying channel impulse response for a diffusion-advection channel is utilized for the first time for odor communication. Finally, the analysis is extended beyond a point-to-point link to inspect the propagation of the alarm signal across a plant population for the first time.

The remainder of this paper is organized as follows. In Section II, the odor pathway in plants is discussed. Section III describes the mathematical framework for the perception of odors by plants. In Section IV, the simulation results are given and discussed. Concluding remarks are given in Section V.

## II. Odor Signalling Pathway in Plants

Plants face many different stresses throughout their life cycles. These can mainly be categorized as biotic and abiotic stresses. Biotic stresses can be caused by insects, bacteria, viruses, fungi, nematodes, arachnids,

Fatih Merdan and O.B. Akan are with the Center for next-generation Communications (CXC), Department of of Electrical and Electronics Engineering, Koç University, Istanbul 34450, Türkiye (e-mail: fmerdan25@ku.edu.tr, akan@ku.edu.tr).

O. B. Akan is also with the Internet of Everything (IoE) Group, Department of Engineering, University of Cambridge, Cambridge CB3 0FA, U.K. (e-mail: oba21@cam.ac.uk).

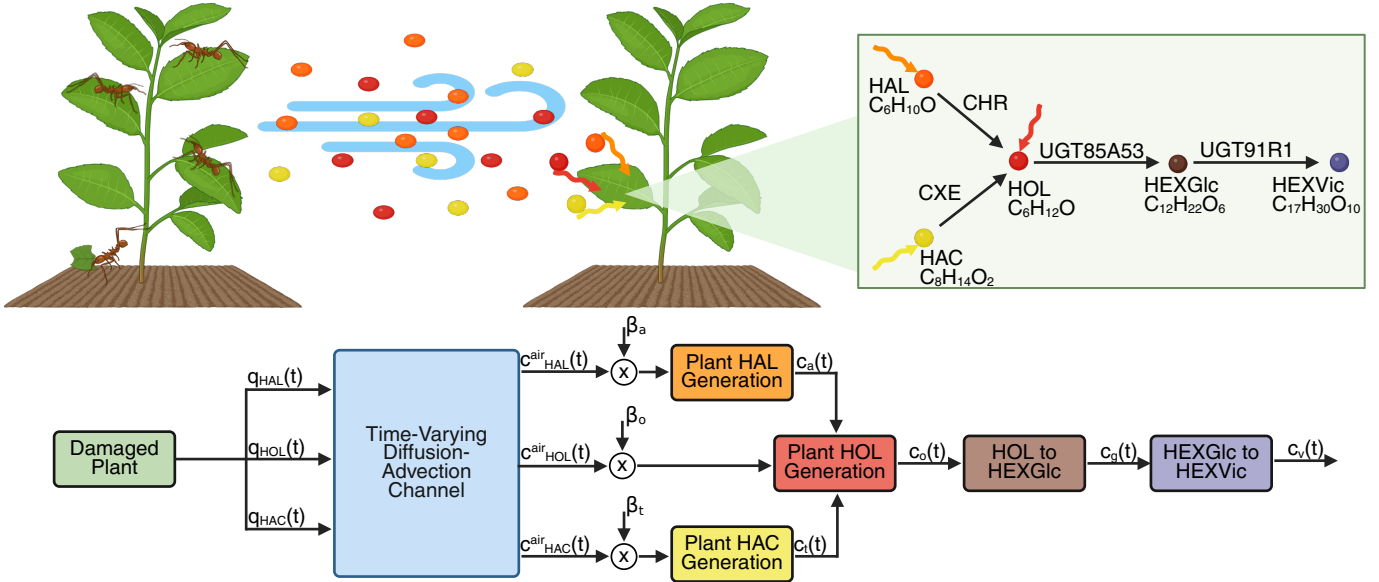


Fig. 1: End-to-end odor communication model used in this work. A damaged plant emits three GLVs (HAL, HOL, and HAC) that propagate through a time-varying diffusion–advection channel. The received air concentrations are subject to multiplicative loss and drive a receiver-side biochemical network (HAL/HAC conversion to HOL and downstream conversion to HEXVic), whose output  $c_v(t)$  is used for the alarm decision [11].

and weeds. Abiotic stresses occur under drought, extreme temperatures, and salinity [12]. As a defense mechanism, plants release Volatile Organic Compounds (VOC) under these stress factors [9]. Stress-induced volatiles are categorized by metabolic origin into four classes: fatty acid degradation products, such as herbivore-induced (Z)-3-hexenol; phenylpropanoids, including cold or drought-induced methyl salicylate (MeSA); biotic and abiotic stress-triggered monoterpenes such as linalool; and sesquiterpenes, such as nerolidol [13]. Green Leaf Volatiles (GLVs) are fatty acid derived Volatile Organic Compounds consisting of six-carbon aldehydes, alcohols, and esters [14]. When the leaves of a plant are physically damaged, GLVs are created on site. Plants can generate substantial amounts of GLVs in seconds to minutes after tissue damage, in some cases reaching nearly  $100 \mu\text{g}$  per gram of fresh weight [15]. They play an important role in the direct defense of plants at wound sites and in indirect plant defense where plants can use GLVs to attract herbivore predators and establish stress communication between neighbouring plants [16], [17].

In this study, GLV transduction is modelled between stressed and unstressed plants. The stressed plant is considered the source of GLVs, and the neighbouring plants are the sinks. Specifically, herbivores feed on the source plant, and with each bite, a new plume of GLVs is released into the air. Green leaf volatile biosynthesis initiates with the formation of (Z)-3-hexenal, which is partially reduced to (Z)-3-hexenol and subsequently acetylated by a BAHD acyltransferase to yield (Z)-3-hexenyl acetate [18], [14]. (Z)-3-hexenal is an aldehyde, (Z)-3-hexenol is an alcohol, and (Z)-3-hexenyl acetate is an ester, and it is possible to transform these into one another.

After the GLVs are released into the atmosphere, they move through a diffusion-advection channel before reaching a GLV sink plant. Particle transport in flowing media arises from both diffusion and advection; however, advection dominates at the macroscale. In nature, the open air is not controlled, and the variations in wind velocity over time are modelled using stochastic signals [19].

When the released GLVs reach a GLV sink plant, they are taken by the leaves of the plant. The general route of gas exchange in plants is through the stomata, which transport  $H_2O$ ,  $CO_2$ , and  $O_2$ . There is also evidence that GLVs are absorbed through the stomata. Adsorption on the cuticle or outer surface of the leaf is another pathway for the intake of GLV by plants [18]. Continuous uptake through the stomata followed by metabolic conversion is the most effective VOC intake pathway, as adsorption is considerably slower than stomatal absorption [20]. This also means that the ability of plants to perceive odor molecules is highly restricted when the stomata of plants are closed, such as in the dark or under drought stress [21]. When the stomata are open, the GLVs first cross the turbulent and leaf boundary layers, enter the stomata, and diffuse into intercellular air spaces. They then undergo air–liquid partitioning, a process governed by Henry’s law constant. In the end, they reach a metabolic site in the leaf. Here, both (Z)-3-hexenal and (Z)-3-hexenyl acetate are transformed into (Z)-3-hexenol. At the same time, (Z)-3-hexenol is processed into (Z)-3-Hexenyl- $\beta$ -D-glucopyranoside (HEXGlc). Finally, HexGlc is converted to (Z)-3-hexenyl  $\beta$ -vicianoside (HEXVic). It has been experimentally shown that HEXVic accumulating leaves are more resilient against herbivore attacks [22]. This

confirms that odor transmission is used for stress communication in plants in nature. This paper focuses on HEXVic accumulation in GLV sink plants after GLV transmission from damaged GLV source plants. However, the effects of GLVs are not limited to HEXVic accumulation. For example, (Z)-3-hexenal exposure results in a  $Ca_{cyt}^{2+}$  increase in guard cells and subsequently in mesophyll cells that trigger the expression of biotic and abiotic stress-responsive genes in a  $Ca^{2+}$  dependent manner [23]. Moreover, it is revealed that exposure to (Z)-3-hexenyl acetate induces ROS Production in Wheat [24]. Both  $Ca^{2+}$  and ROS are important secondary signals in plants that can activate many defense-related enzymes, and future research is needed to uncover their mechanics.

### III. Odor Perception Dynamics in Plants

In a communication paradigm, there are three main elements: the transmitter, the receiver, and the channel. In this section, odor signalling between plants is characterized by mathematically defining these elements together with the relevant signals. The proposed model for the odor perception by plants is given in Fig. 1.

Due to the absence of a comprehensive dataset for a single species, biological parameters were aggregated from multiple plant sources to parameterize the system. Nevertheless, since all of these species exhibit odor perception, the resulting framework can be regarded as a general plant model for odor sensing. In addition, all odor molecules are assumed to be processed within a single effective cytosolic volume, and the corresponding enzyme concentrations are computed on the same basis.

#### A. Odor Transmitter

The transmitter plant releases (Z)-3-hexenal (HAL), (Z)-3-hexenol (HOL), and (Z)-3-hexenyl acetate (HAC) due to herbivore damage. Each bite of the leaf is represented as a bit. Bit 0 corresponds to no bite, where there is no GLV emission, and bit 1 corresponds to a bite. The release of GLVs into the air is modelled as a rectangular pulse of length 2 seconds. The emission amplitudes of each odor molecule are determined from [25] using the data from the cut leaves of the corn plant and given in Table II. The transmitted signal is described as

$$q(t) = \sum_{k=1}^N A_m p(t - kT_{sym}), \quad (1)$$

where  $A_m$  is the emission amplitude of the odor molecule,  $T_{sym}$  is the symbol period, and  $p(t)$  is a rectangular pulse of length  $T_{sym}$ . Although proper bit and symbol definitions are made, plants are not able to reconstruct these bits. Eventually, the released GLVs will be understood as an alarm signal only.

#### B. Diffusion-Advection Channel

The movement of odor particles in the air is described with a partial differential equation as

$$\frac{\partial c}{\partial t}(\mathbf{x}, t) = D\nabla^2 c(\mathbf{x}, t) - \mathbf{v}(t) \cdot \nabla c(\mathbf{x}, t) + S(\mathbf{x}, t), \quad (2)$$

where  $c(\mathbf{x}, t)$  denotes the concentration of the particle at position  $\mathbf{x}$  and time  $t$ ,  $D$  is the constant air diffusion coefficient,  $\mathbf{v}(t)$  is the wind velocity vector,  $\nabla c(\mathbf{x}, t)$  and  $\nabla^2 c(\mathbf{x}, t)$  represent the spatial gradient and Laplacian of the concentration, respectively, and  $S(\mathbf{x}, t)$  denotes the transmitter plant. The time-varying diffusion-advection channel impulse response described in [26] is used to accurately model the movements of GLVs under a time-varying diffusion-advection channel. To do this, the transmitter plant is modelled as a point source as  $S(\mathbf{x}, t) = q(t)\delta(\mathbf{x} - \mathbf{x}_0)$  where  $\mathbf{x}_0$  is the transmitter plant position and the initial zero condition is assumed for each odor molecule.

The air diffusion coefficients for each molecule are calculated using the Fuller method explained in [27]. The output of the channel is the concentration of the odor molecules around a receiver plant position.

#### C. Odor Receiver

Receivers are also modeled as points in a 3-D space, and it is assumed that the stomata of the receiver plants remain open throughout the communication process. The air concentrations of HAL, HOL, and HAC are the input of the receiver. The receiver plant first absorbs the odor molecules from the air. Then, these are metabolized into HEXVic through enzymatic reactions. The receiver decides that there is an attack nearby if the concentration of HEXVic in the leaves  $c_v(t)$  passes through a threshold  $c_{v0}$ . Therefore, the amount of HEXVic accumulated in the leaf is used as the main output of the system.

1) Random Multiplicative Loss: Within the receiver leaf, not all absorbed odor molecules are utilized by the targeted biochemical pathway. A portion of these molecules may be sequestered in other plant tissues or consumed by competing metabolic reactions. Furthermore, the successful interaction between a molecule and its corresponding enzyme at the reaction site is inherently stochastic, depending on the probability of molecular collision [28]. In addition, it is found that certain herbivores release salivary enzymes that suppress GLV emissions from the source plant [29]. These physical and biochemical uncertainties are collectively modeled at the receiver input through a random multiplicative loss factor.

To model the loss factors for HAL, HAC, and HOL, Beta-distributed random variables that are independent across time samples are employed. The specific profile of each loss factor is characterized by its mean and coefficient of variation (CV) [30], tailored to each molecule type. This framework serves as a biological analog to Signal-to-Noise Ratio (SNR) control in classical communication systems: the mean of the distribution scales the effective input amplitude, while the CV dictates the magnitude of stochastic fluctuations that degrade detection reliability.

2) Odor Absorption: Using the definitions in [20], VOC absorption by plant leaves is mathematically modelled as

$$\left(\frac{r_{ias}}{F} + \frac{1}{\left(\frac{1}{r_G} + \frac{E}{2}\right)} + \frac{10^3 r_{liq}}{HP_a}\right)A = \left(\frac{\frac{1}{r_G} - \frac{E}{2}}{\left(\frac{1}{r_G} + \frac{E}{2}\right)}\right)C_a - \frac{10^3}{HP_a}C_{ct}, \quad (3)$$

where  $r_{ias} = \frac{\Delta L_{ias}\tau}{D_A f_{ias}}$  is the intercellular airspace resistance,  $\Delta L_{ias}$  is the effective diffusion path length in intercellular air spaces,  $\tau$  is the diffusion path tortuosity,  $D_A$  is the diffusion coefficient of VOC in gas phase and  $f_{ias}$  is the fraction of the intercellular air space volume in the total leaf volume.  $F = \frac{273.15}{T_k \times 22.4e-3}$  is a scaling constant where  $T_k$  is the temperature in *kelvin*.  $r_G = r_s + r_b$  is the total resistance from outside air to intercellular air spaces.  $r_b = r_b^w \left(\frac{D_w}{D_A}\right)^{\frac{2}{3}}$  is the resistance of the leaf boundary layer, where  $r_b^w$  is the resistance of the leaf boundary layer for water vapor and  $D_w$  is the diffusion coefficient of water in the gas phase. Similarly,  $r_s = r_s^w \left(\frac{D_w}{D_A}\right)$  is the stomatal resistance and  $r_s^w$  is the stomatal resistance for water vapor.  $E$  is the VOC specific transpiration rate,  $H$  is the VOC specific Henry's constant taken from [25] and  $P_a$  is the pressure in *bar*.  $r_{liq}$  is the sum of the resistances of the cell wall, plasma membrane, and cytosol. It is calculated following the description given in [20] for each odor molecule. To do this, the parameters of the plant *Spathiphyllum clevelandii* are used. Moreover, the Octanol/Water partition coefficients ( $K_{o/w}$ ) for the odor molecules are obtained from the Chemo database [31]–[33].

In (3),  $A$  is the odor molecule absorption rate in  $mol\ m^{-2}\ s^{-1}$ ,  $C_a$  is the odor concentration in the atmosphere in *ppb* and  $C_{ct}$  is the odor concentration in cytosol in  $mol\ m^{-3}$ . In this equation,  $C_a$  and  $C_{ct}$  are known, and  $A$  is the output at a time instant. The output of the channel is in  $mol/m^3$ . To convert the unit of  $C_a$  from  $mol/m^3$  to *ppb*, the methods explained in [34] and [35] are utilized. Since in the receiver, *molar* absorption rates are used,  $A$  is converted into  $mol\ L^{-1}\ s^{-1}$  as

$$A(mol\ L^{-1}\ s^{-1}) = A(mol\ m^{-2}\ s^{-1}) \times \frac{LA_{FW}}{V_{intra}}, \quad (4)$$

where  $LA_{FW}$  is the leaf area per fresh weight ( $m^2\ g^{-1}\ FW$ ) obtained from [36] and  $V_{intra}$  is the water volume of leaf tissue per unit fresh weight ( $L\ g^{-1}\ FW$ ). Using the fact that *Arabidopsis* leaves normally has  $0.90\ g\ g^{-1}\ FW$  [37], and taking the density of water  $1\ g/ml$ ,  $V_{intra}$  is calculated.

3) HAL to HOL Conversion: Absorbed HAL inside the leaves ( $c_a(t)$ ) is processed into HOL. In [16], the enzyme encoded by At4g37980 in *Arabidopsis* is shown to convert HAL into HOL, and is named as CHR. To represent this chemical reaction, Michaelis-Menten Equations are used [38]. The rate of change from HAL to HOL is represented as

$$J_{AO}(t) = k_{cat}^{ao} E_{CHR} \frac{c_a(t)}{k_m^{ao} + c_a(t)}, \quad (5)$$

where  $k_{cat}^{ao}$  is the catalytic constant,  $E_{CHR}$  is the total CHR concentration in the leaf,  $k_m^{ao}$  is the Michaelis

constant for this reaction and  $c_a(t)$  is the total cytosolic HAL concentration in the leaf.

4) HAC to HOL Conversion: As reported in [39], the *Arabidopsis* enzyme AtCXE12 is shown to metabolize HAC into HOL. To model this reaction, a similar Michaelis-Menten dynamics is used as

$$J_{TO}(t) = k_{cat}^{to} E_{CXE} \frac{c_t(t)}{k_m^{to} + c_t(t)}, \quad (6)$$

where  $E_{CXE}$  is the total AtCXE12 concentration in the leaf, and  $c_t(t)$  is the total cytosolic HAC concentration in the leaf.

5) HOL to HEXGlc Conversion: According to [40], the UGT85A53 protein in *Camellia sinensis* is responsible for HEXGlc accumulation from airborne HOL. A Michaelis-Menten dynamics is used as

$$J_{OG}(t) = k_{cat}^{og} E_{85A} \frac{c_o(t)}{k_m^{og} + c_o(t)}, \quad (7)$$

where  $E_{85A}$  is the total UGT85A53 concentration in the leaf, and  $c_o(t)$  is the total cytosolic HOL concentration in the leaf.

6) HEXGlc to HEXVic Conversion: Evidence in [41] shows that the enzyme UGT91R1 mediates HEXVic accumulation in *S. lycopersicum* by preferentially catalyzing the arabinosylation for HEXGlc. Similarly, this dynamic is modelled as

$$J_{GV}(t) = k_{cat}^{gv} E_{91R} \frac{c_g(t)}{k_m^{gv} + c_g(t)}, \quad (8)$$

where  $E_{91R}$  is the total UGT91R1 concentration in the leaf, and  $c_g(t)$  is the total cytosolic HEXGlc concentration in the leaf.  $c_v(t)$  is used to represent the total cytosolic HEXVic concentration.

Using the method explained in [42], the total enzyme concentrations from *ppm* values can be found as

$$E_{tot} = \frac{k_e A_b 10^{15}}{N_A}, \quad (9)$$

where  $k_e \approx 3e6$  is an estimate of cellular density of protein molecules per *femtoliter*,  $A_b$  is the abundance, and  $N_A$  is the Avogadro constant. The abundance values of the enzymes are obtained from the PaxDb database [43]. For AtCXE12 and CHR, the *Arabidopsis* leaf tissue is used. For UGT85A53, the *Arabidopsis* gene UGT85A1, and for UGT91R1, the *Arabidopsis* gene UGT91A1 is used, with the abundance in the whole organism.

Using the absorption rates from (4) and the enzymatic rates from (5), (6), (7), and (8) the following

TABLE I: Biological-Chemical Parameters

Description	Symbol	Value	Unit	Description	Symbol	Value	Unit
Temperature	$T_k$	298.15	<i>kelvin</i>	Diffusion path tortuosity	$\tau$	1.57	$mm^{-1}$
Pressure	$P$	1	<i>atm</i>	Fraction of the intercellular air space volume in the total leaf volume	$f_{ias}$	0.328	$m^3 m^{-3}$
Molecular weight of HAL	$M_a$	98.143	<i>g/mol</i>	Henry's constant (HAL)	$H_a$	6.0	$mol L^{-1} atm^{-1}$
Molecular weight of HOL	$M_o$	100.159	<i>g/mol</i>	Henry's constant (HOL)	$H_o$	113	$mol L^{-1} atm^{-1}$
Molecular weight of HAC	$M_t$	142.2	<i>g/mol</i>	Henry's constant (HAC)	$H_t$	3.1	$mol L^{-1} atm^{-1}$
Molecular weight of vapor	$M_w$	18	<i>g/mol</i>	Octanol/Water partition coefficient (HAL)	$K_{o/w}^a$	$10^{1.542}$	-
Diffusion coefficient of HAL	$D_a$	$8.0718 \times 10^{-6}$	$m^2/s$	Octanol/Water partition coefficient (HOL)	$K_{o/w}^o$	$10^{1.335}$	-
Diffusion coefficient of HOL	$D_o$	$7.9291 \times 10^{-6}$	$m^2/s$	Octanol/Water partition coefficient (HAC)	$K_{o/w}^t$	$10^{1.906}$	-
Diffusion coefficient of HAC	$D_t$	$6.7698 \times 10^{-6}$	$m^2/s$	Abundance of CHR	$A_b^{CHR}$	330	<i>ppm</i>
Diffusion coefficient of vapor	$D_w$	$2.3289 \times 10^{-5}$	$m^2/s$	Abundance of AtCXE12	$A_b^{CXE}$	122	<i>ppm</i>
Leaf area per fresh weight	$LA_{FW}$	0.0055	$m^2 g^{-1} FW$	Abundance of UGT85A53	$A_b^{85A}$	13.2	<i>ppm</i>
water volume of leaf tissue per unit fresh weight	$V_{intra}$	0.0009	$L g^{-1} FW$	Abundance of UGT91R1	$A_b^{91R}$	0.09	<i>ppm</i>
Leaf boundary layer resistance for water vapor (HAL)	$r_{b_a}^w$	2.58	$m^2 s/mol$	Avogadro constant	$N_A$	$6.02 \times 10^{23}$	$mol^{-1}$
Stomatal resistance for water vapor (HAL)	$r_{s_a}^w$	21.8	$m^2 s/mol$	Catalytic constant (CHR)	$k_{cat}^{ao}$	13.27	$s^{-1}$
Leaf boundary layer resistance for water vapor (HOL)	$r_{b_o}^w$	3.23	$m^2 s/mol$	Catalytic constant (CXE)	$k_{cat}^{to}$	3.78	$s^{-1}$
Stomatal resistance for water vapor (HOL)	$r_{s_o}^w$	26.5	$m^2 s/mol$	Catalytic constant (85A)	$k_{cat}^{og}$	0.35	$s^{-1}$
Leaf boundary layer resistance for water vapor (HAC)	$r_{b_t}^w$	2.47	$m^2 s/mol$	Catalytic constant (91R)	$k_{cat}^{gv}$	0.33	$s^{-1}$
Stomatal resistance for water vapor (HAC)	$r_{s_t}^w$	16.1	$m^2 s/mol$	Michaelis constant (CHR)	$k_m^{ao}$	32.7	$\mu M$
HAL transpiration rate	$E_a$	$6 \times 10^{-4}$	$mol m^{-2} s^{-1}$	Michaelis constant (CXE)	$k_m^{to}$	5940	$\mu M$
HOL transpiration rate	$E_o$	$5.4 \times 10^{-4}$	$mol m^{-2} s^{-1}$	Michaelis constant (85A)	$k_m^{og}$	18.92	$\mu M$
HAC transpiration rate	$E_t$	$4.5 \times 10^{-4}$	$mol m^{-2} s^{-1}$	Michaelis constant (91R)	$k_m^{gv}$	5.9	$\mu M$
Effective diffusion path length in intercellular air spaces	$\Delta L_{ias}$	$6.38 \times 10^{-5}$	<i>m</i>				

system of differential equations is constructed

$$\begin{aligned}
\frac{dc_a(t)}{dt} &= A_a(t) - J_{AO}(t), \\
\frac{dc_t(t)}{dt} &= A_t(t) - J_{TO}(t), \\
\frac{dc_o(t)}{dt} &= A_o(t) + J_{AO}(t) + J_{TO}(t) - J_{OG}(t), \quad (10) \\
\frac{dc_g(t)}{dt} &= J_{OG}(t) - J_{GV}(t), \\
\frac{dc_v(t)}{dt} &= J_{GV}(t).
\end{aligned}$$

where  $A_a(t)$ ,  $A_o(t)$ , and  $A_t(t)$  are the absorption rates of HAL, HOL, and HAC, respectively. All biological-chemical parameters are given in Table I.

#### IV. Simulation Results

In this Section, numerical analysis of the given topology is carried out. First, the receiver characteristics are inspected in detail. Then, the end-to-end communication system is inspected between one transmitter and one receiver plant. Lastly, the distribution of the alarm signal is analyzed across a comprehensive set of receiver

coordinates to characterize how the warning message is perceived by the surrounding plant population under different wind conditions. For multi-receiver scenarios, the channel is simulated in Python using an NVIDIA GeForce GTX 1080 Ti GPU, and the channel output is saved. Subsequent analysis is conducted using MATLAB R2023b. The parameters used in the simulations are given in Table II.

##### A. Receiver Characteristics

The odor receiver presented in this work is designed to study the initial stimulation phase of the receiver plant. Because the model does not yet include a 'reset' or recovery mechanism, it continuously accumulates incoming signals. This receiver can be taken as a linear time invariant (LTI) system if for each enzymatic reaction  $k_m \gg c(t)$  is satisfied. It can be observed that, as long as the receiver keeps getting an input, it will leave the linear operating region because the internal concentrations will increase as time progresses. To understand the linearity limits of this system with respect to its 3 inputs, a practical method is introduced. Specifically, if for that simulation duration, the time fraction for which  $r > 0.1$  is less than

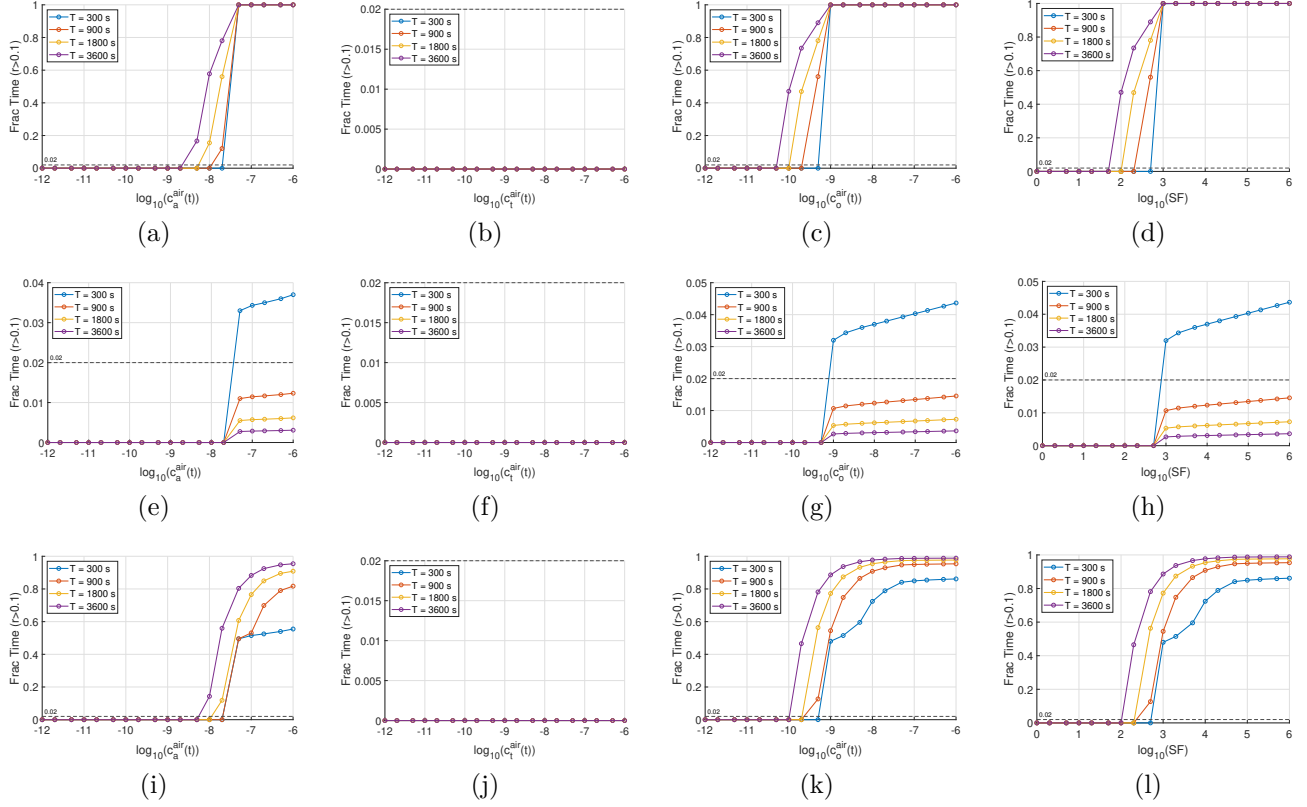


Fig. 2: Receiver nonlinearity results across various simulation times, input signal configurations, and scaling scenarios. For (i) constant inputs (a) scales HAL only, (b) scales HAC only, (c) scales HOL only, and (d) scales all three input amplitudes together, and the horizontal axis shows the common scaling factor (SF). For (ii) single initial pulses, (e) scales HAL only, (f) scales HAC only, (g) scales HOL only, and (h) scales all three input amplitudes together. For (iii) periodic on-off cycling, (i) scales HAL only, (j) scales HAC only, (k) scales HOL only, and (l) scales all three input amplitudes together. The horizontal dashed lines indicate the 0.02 threshold used to define the LTI operating region.

or equal to 0.02, the system is treated as operating in the linear regime, where

$$r = \max\left(\frac{c_a(t)}{k_m^{ao}}, \frac{c_t(t)}{k_m^{to}}, \frac{c_o(t)}{k_m^{og}}, \frac{c_g(t)}{k_m^{gv}}\right). \quad (11)$$

The linearity condition is evaluated across various simulation durations and input signal profiles. In each configuration, the amplitude of one input signal is increased while the other two are held constant to examine the linearity; subsequently, all three input amplitudes are simultaneously increased to observe the collective behavior. For all cases, the initial air concentrations of each odor molecule are set to  $1 \times 10^{-12} \text{ mol/m}^3$ . Three input signal configurations are evaluated: (i) a constant input, (ii) a single initial pulse ( $T_{on} = 10\text{s}$ ), and (iii) periodic on-off cycling ( $T_{on} = T_{off} = 10\text{s}$ ). The results are presented in Fig. 2. As expected, for both constant and periodic on-off cycling input profiles, the minimum input amplitude required to exceed the linearity threshold decreases as simulation duration increases. In the case of a single initial pulse, the specific amplitude at which linearity breaks can be identified for each odor molecule. Notably, the system exhibits a return to the linear regime

as time progresses in this configuration. This recovery occurs because the concentrations of molecules responsible for breaking linearity decrease over time as they are converted into downstream metabolites like HEXGlc. Across all configurations, the results for HOL scaling and simultaneous scaling are nearly identical, implying that HOL is the primary limiter of the linear operating region. In contrast, HAC remains within the linear regime across all tested scenarios and durations.

To study the frequency characteristics of the odor receiver, the magnitude and phase response of the system are evaluated. Since the input signals correspond to concentration levels, they cannot be negative. Therefore, the oscillating inputs are given to the system in the form shown as

$$c_x^{air}(t) = A(1 + \cos(2\pi ft)), \quad (12)$$

where  $A = 5 \times 10^{-11} \text{ mol/m}^3$  corresponds to a linear operation region according to Fig. 2. In each simulation, only one input is made oscillatory, and the other two are taken as zero. To be able to work with oscillating outputs once there are oscillating inputs, the output of the system is considered as the internal plant HOL concentration

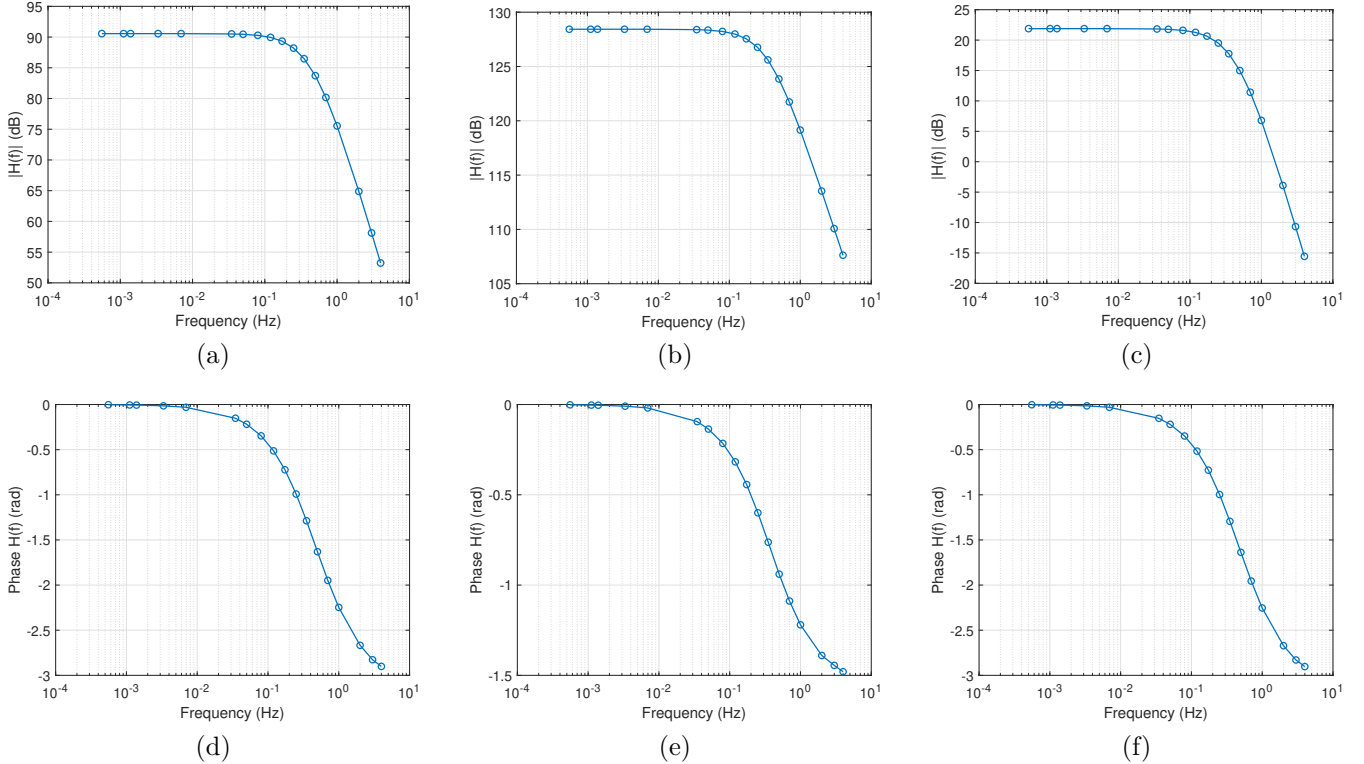


Fig. 3: Frequency-domain response of the HOL output to different odor inputs. The top row shows the magnitude responses for HAL, HOL, and HAC inputs in (a), (b), and (c), respectively. The bottom row presents the corresponding phase responses in (d), (e), and (f).

( $c_o(t)$ ) in this analysis. In general, the output is of the form  $c_o(t) = B(1 + \cos(2\pi ft + \phi))$ , where  $B$  has units  $\mu\text{mol}/L$ . Then, the frequency response of the system is calculated as

$$H(t) = \frac{Be^{j\phi}}{A[\mu\text{mol}/L]}. \quad (13)$$

Using these definitions, the magnitude and phase response of the system are calculated and given in Fig. 3. The results show that the magnitude response remains constant at low frequencies and begins to roll off as the frequency increases for each odor molecule. This indicates that the plant’s biochemical network cannot track rapid fluctuations in odor concentration. Moreover, the effective bandwidth of the biological receiver appears consistent across all three odor molecules. This suggests that the rate-limiting step in the biochemical network is likely common to all three pathways, potentially the final conversion stages leading to the HOL concentration. In addition, there is a significant difference in the magnitude response among the three inputs. HOL exhibits the highest gain, while HAC has the lowest gain. These findings confirm the observation that HOL is the dominant driver for this system.

To understand the sensitivity of the linear operation region to the enzyme abundances, the abundances of UGT85A53 and UGT91R1 are varied, and the linearity is examined. For this analysis, periodic on-off cycling input

is applied for 1 *hour*, and the results are given in Fig. 4. It can be observed that the system’s linearity is significantly more sensitive to the abundance of UGT85A53. This result further demonstrates that HOL is the critical odor molecule for the receiver, as its conversion process represents the primary constraint on the system’s ability to maintain a linear response.

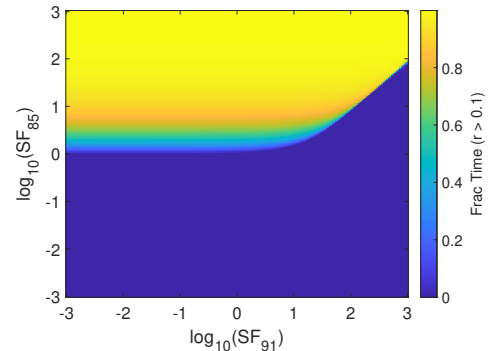


Fig. 4: Sensitivity analysis of the linear operating region with respect to enzyme abundances. The horizontal and vertical axes show the scaling factors for each enzyme abundance.

## B. End-to-End Communication System

Here, the end-to-end communication system is simulated using a single transmitter-receiver plant pair. In

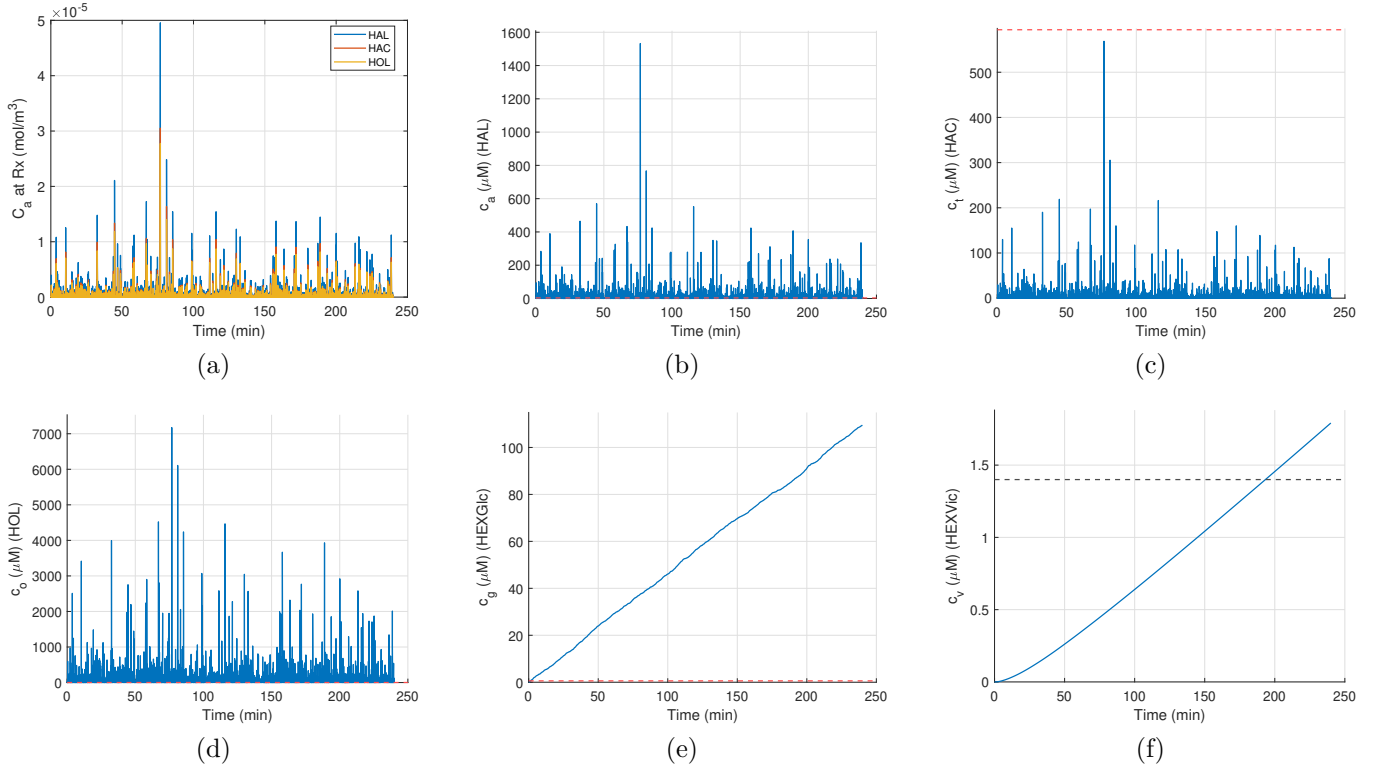


Fig. 5: 1-transmitter 1-receiver simulation results. The channel output air concentrations are shown in (a). The internal leaf concentrations are shown for (b) HAL, (c) HAC, (d) HOL, (e) HEXGlc, and (f) HEXVic. The red dashed lines indicate the linearity limit for that molecule, and the black dashed line indicates the alarm decision threshold.

these simulations, equiprobable insect bites (bits) are used. The propagation channel is simulated independently for the three considered GLVs using a shared wind realization, under the assumption that the molecules do not interact or affect one another's movement. For each receiver position and for each odor molecule, (2) is solved. In addition, zero-mean white Gaussian wind is assumed for the  $x$  and  $y$  dimensions, while there is no wind in the  $z$  dimension. In [22], a comprehensive metabolite analysis of leaf extracts is conducted, and the amount of HEXVic was found to be  $0.10 \pm 0.02 \mu\text{g.g}^{-1}FW$  in control plants, and  $2.39 \pm 0.78 \mu\text{g.g}^{-1}FW$  in plants exposed to volatiles from neighboring herbivore-infested plants. In accordance with this, the alarm threshold in this article is taken as  $0.5 \mu\text{g.g}^{-1}FW$ . Using the molecular weight of HEXVic ( $MW_v = 394.4 \text{g/mol}$ ), the threshold is written in units  $\mu M$  as

$$c_{v0} [\mu M] = \frac{c_{v0} [\mu\text{g.g}^{-1}FW] \times 10^{-3}}{MW_v \times V_{intra}}. \quad (14)$$

Parameters described in Table II for a non-directed strong wind scenario are used, and important signals are plotted. These results are given in Fig. 5. It is observed that the receiver works in the non-linear region of operation in a general natural setting. As can be seen in Fig. 5(a), there is no bit-wise structure due to the channel effects. However, the receiver plant is able to obtain the information that "there is an attack nearby".

From the previous receiver analysis, it was found that the input HOL air concentration is the strongest signal that contributes to the output internal HEXVic concentration. However, understanding the individual effects of HAL, HOL, and HAC from the perspective of communication engineering requires the main operations in the transmitter plant as well. In this article, the Carbon concentration budgeted idea is introduced. Using the emission amplitudes given in Table II, the maximum Carbon molecule emission amplitude is determined as  $3.728 \times 10^{-10} \text{mol/s}$ . Then, this amount is used to send only one type of GLV per simulation with emission amplitudes  $A_a = A_o = 6.21 \times 10^{-11} \text{mol/s}$  and  $A_t = 4.66 \times 10^{-11} \text{mol/s}$ . For this analysis, the parameters in Table II for the directed wind scenario are used, and the resulting plot is given in Fig. 6. This result also suggests that HOL is the most efficient molecule to transmit. Then, a natural question arises: Why do plants send different GLVs, and not only HOL with higher amounts? To properly answer this question, one needs to develop a way to characterize the energy required to produce and store these molecules in a transmitter plant. Furthermore, one has to take into account the fact that storage of one molecule in large amounts can be toxic to the plant [16], [15]. Therefore, toxicity limits for these molecules must be established. These questions motivate a multidisciplinary research direction that requires close collaboration between engineers and biologists.

TABLE II: Simulation Parameters

Description	Value
Timing and decision	
Channel sampling rate, $f_s$	10 Hz
Symbol duration, $T_{\text{sym}}$	2 s
HEXVic alarm threshold, $c_{v0}$	1.4 $\mu\text{M}$
Receiver-side multiplicative loss	
Beta-loss (HAL/HAC/HOL)	mean, 0.85
Beta-loss coefficient of variation (CV)	0.15
Emission amplitudes	
HAL emission amplitude, $A_a$	$2.76 \times 10^{-11}$ mol/s
HOL emission amplitude, $A_o$	$1.52 \times 10^{-11}$ mol/s
HAC emission amplitude, $A_t$	$1.45 \times 10^{-11}$ mol/s
Geometry	
Tx position	[0, 0, 1] m
Rx position (1Tx-1Rx)	[0.15, 0, 1] m
Rx position (GLV comparison)	[0.20, 0, 1] m
Wind regimes	
Non-directed strong wind	$\mu_x = \mu_y = 0$ m/s, $\sigma_x = \sigma_y = 0.5$ m/s
Non-directed weak wind	$\mu_x = \mu_y = 0$ m/s, $\sigma_x = \sigma_y = 0.01$ m/s
Directed wind	$\mu_x = 0.2$ , $\mu_y = 0$ m/s, $\sigma_x = \sigma_y = 0.01$ m/s

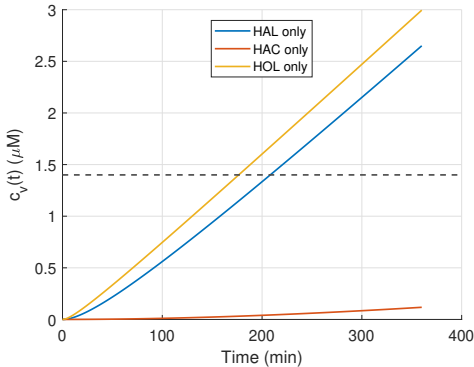


Fig. 6: Comparison of internal HEXVic accumulation for single GLV emission scenarios.

One possible explanation for the usage of multiple odor molecules can be given from a communication theoretical perspective. Here, the plant is transmitting the same message over independent channels. This can be thought of as a form of diversity combining technique. We name this technique chemical diversity combining. Chemical diversity combining does not improve the accuracy of communication by somehow overcoming the effects of the diffusion-advection channel. As can be seen in Fig. 5(a), all odor molecules travel in the air in a similar manner. That is, the wind determines the movements. Therefore, odor molecules having different masses or diffusion coefficients do not matter in this topology. Chemical diversity combining can increase the accuracy of communication by introducing different, preferably independent, chemical

channels for the same outcome. For example, insects that feed on a leaf can release salivary enzymes that suppress HOL emission from that leaf, but HAL and HAC can still be emitted. Or, the receiver plant might be in such a state that it must use HAL for different chemical reactions. In these kinds of scenarios, utilizing chemical diversity by combining techniques by sending the same message over different chemical channels can prove helpful for the communication link.

Since the receiver is an accumulator, the meaningful metric to consider in this topology to quantify the communication is the time at which the receiver plant becomes "alarmed". This time is referred to as Alarm Time. The odor communication link between a single transmitter-receiver pair is further analyzed by inspecting the alarm time in different wind scenarios at different distances. Here, distance refers to the  $x$ -axis position of the receiver plant. In addition, the initial time where the receiver becomes non-linear, referred to as Linearity Time, is also inspected. The simulation results for these analyses are presented in Fig. 7. The results show that the alarm time increases with increasing distance for all wind regimes. Wind variability significantly affects this trend: while the directed-wind case yields a smooth and predictable increase, the non-directed regimes exhibit stronger distance sensitivity and non-smooth transitions. For the non-directed weak wind scenario, after  $1m$ , the receiver plants do not get any message. Comparing linearity and alarm times reveals that the alarm decision typically occurs while the receiver operates in the non-linear region.

### C. Spread of the Alarm Message

Here, how the warning message is received by the surrounding population is simulated. Many receiver plants are placed around one transmitter plant. The simulations are carried out for the non-directed strong wind and non-directed weak wind scenarios, assuming that the stomata of all plants are open throughout the simulation. The results are given in Fig. 8. It is observed that, under the non-directed strong wind scenario, the alarm message propagates significantly further from the transmitter. In contrast, under weak wind conditions, the alarm remains largely localized. This result, together with the results of Fig. 7, shows how the communication of the alarm message is highly dependent on the strong carrier wind. This dependency suggests a direct application in the design of automated monitoring systems for smart greenhouses. Specifically, integrating controlled airflow management can optimize signal coverage and reduce detection latency, ensuring that localized pest or pathogen outbreaks are rapidly communicated to the entire plant population and monitoring devices through the diffusion-advection channel. By maintaining a consistent medium flow, the communication radius of the biological receivers can be artificially extended, facilitating more robust and predictable bio-monitoring networks.

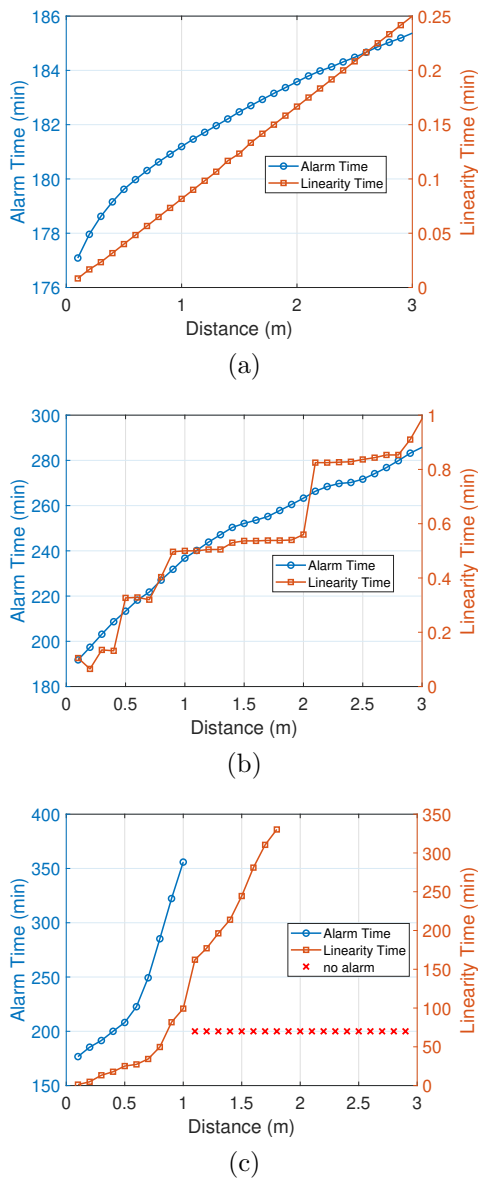


Fig. 7: Alarm time and linearity time versus Tx-Rx distance for three wind regimes: (a) directed wind, (b) non-directed strong wind, and (c) non-directed weak wind.

## V. Conclusion

This study presents a comprehensive end-to-end communication model for odor signaling in plants, specifically focusing on the transduction of GLVs from stressed source plants to unstressed sink plants. By integrating diffusion-advection channel dynamics with a receiver-side biochemical network, the transformation of airborne (Z)-3-hexenal (HAL), (Z)-3-hexenol (HOL), and (Z)-3-hexenyl acetate (HAC) into the defensive metabolite (Z)-3-hexenyl  $\beta$ -vicianoside (HEXVic) is characterized. Notably, HOL was identified as the primary driver of the system and the main constraint on the receiver's linear operating region. This specific technical insight opens a deeper inquiry into the evolutionary logic of plant behavior: why has the utilization of a diverse composition of molecules

evolved if a single component serves as the primary driver? By synthesizing engineering principles with biological systems, these complex signaling trade-offs can be decoded as optimized information-sharing strategies.

It is emphasized that the restriction of the stomata limits the capacity for odor communication, suggesting that future smart agriculture techniques should rely on hybrid systems that incorporate various biological signals. Although plants may not be able to decode the full bit sequence of a stress event, specialized devices could be developed to extract more detailed data, such as specific herbivore biting patterns. This hidden information could be reconstructed to allow highly informed decisions in agriculture applications.

To build on these findings, future studies should aim to uncover the mechanics of other secondary signals, such as  $Ca^{2+}$  and ROS, and incorporate recovery mechanisms to model the long-term "resetting" of the biological receiver. Ultimately, the adoption of this interdisciplinary approach allows the evolutionary background of plant communication to be better understood, while a practical framework is provided to use these biological mechanisms for next-generation precision farming.

## References

- [1] S. M. Westman, K. J. Kloth, J. Hanson, A. B. Ohlsson, and B. R. Albrechtsen, "Defence priming in Arabidopsis – a Meta-Analysis," *Scientific Reports*, vol. 9, no. 1, p. 13309, September 2019.
- [2] A. C. Jones, T. M. Cofer, J. Engelberth, and J. H. Tumlinson, "Herbivorous Caterpillars and the Green Leaf Volatile (GLV) Quandary," *Journal of Chemical Ecology*, vol. 48, no. 3, pp. 337–345, March 2022.
- [3] F. Loreto and S. D'Auria, "How do plants sense volatiles sent by other plants?" *Trends in Plant Science*, vol. 27, no. 1, pp. 29–38, January 2022.
- [4] A. K. Meents and A. Mithöfer, "Plant-Plant Communication: Is There a Role for Volatile Damage-Associated Molecular Patterns?" *Frontiers in Plant Science*, vol. 11, October 2020.
- [5] A. B. Kilic and O. B. Akan, "Information and communication theoretical foundations of the internet of plants, principles, challenges, and future directions," 2025. [Online]. Available: <https://arxiv.org/abs/2509.08434>
- [6] A. Z. Babar and O. B. Akan, "Sustainable and precision agriculture with the internet of everything (ioe)," 2025. [Online]. Available: <https://arxiv.org/abs/2404.06341>
- [7] D. Aktas et al., "Odor-based molecular communications: State-of-the-art, vision, challenges, and frontier directions," *IEEE Communications Surveys & Tutorials*, vol. 27, no. 4, pp. 2658–2692, 2025.
- [8] B. D. Unluturk and I. F. Akyildiz, "An End-to-End Model of Plant Pheromone Channel for Long Range Molecular Communication," *IEEE Transactions on NanoBioscience*, vol. 16, no. 1, pp. 11–20, January 2017.
- [9] A. B. Kilic and O. B. Akan, "End-to-end mathematical modeling of stress communication between plants," *IEEE Transactions on Molecular, Biological, and Multi-Scale Communications*, vol. 12, pp. 69–78, 2026.
- [10] B. Maitra and O. B. Akan, "Modeling and analysis of voc-based interplant molecular communication channel," 2025. [Online]. Available: <https://arxiv.org/abs/2512.12035>
- [11] F. Merdan, "Created in biorender," <https://BioRender.com/z55x3op>, 2026, bioRender Illustration.
- [12] J. Midzi, D. W. Jeffery, U. Baumann, S. Rogiers, S. D. Tyerman, and V. Pagay, "Stress-Induced Volatile Emissions and Signalling in Inter-Plant Communication," *Plants*, vol. 11, no. 19, p. 2566, January 2022.

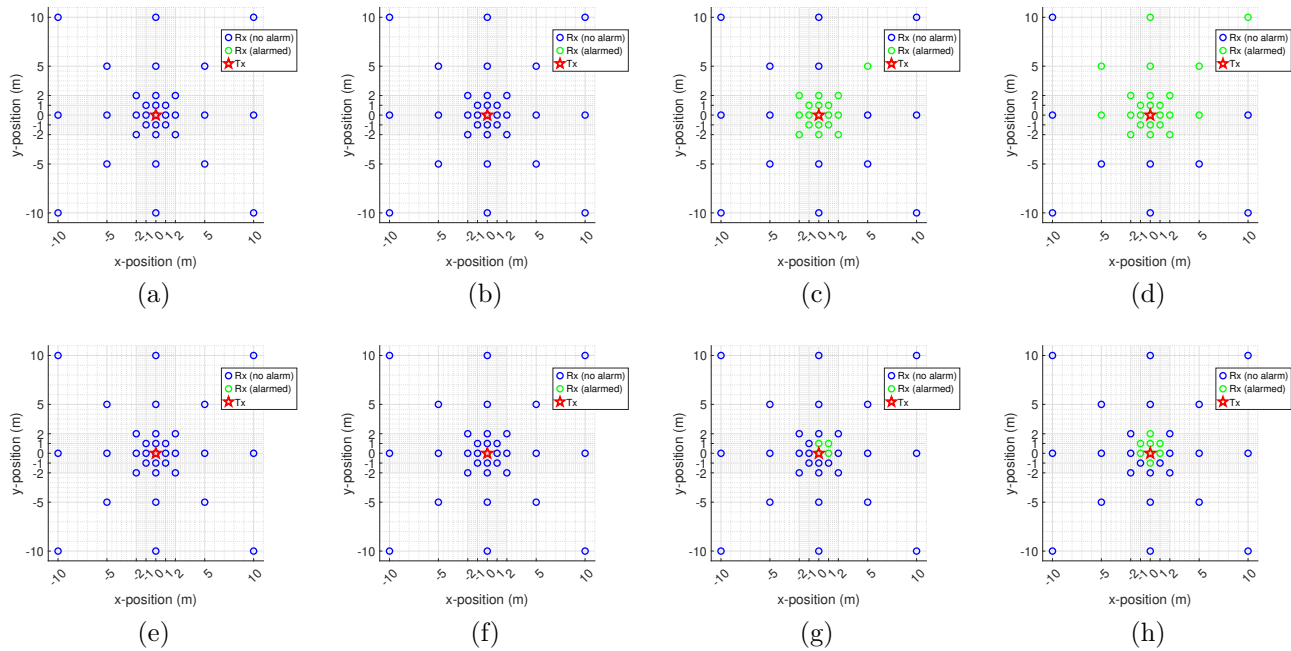


Fig. 8: Population-level alarm maps under non-directed strong wind after (a) 1 hour, (b) 3 hours, (c) 6 hours, and (d) 10 hours, and the maps under non-directed weak wind after (e) 1 hour, (f) 3 hours, (g) 6 hours, and (h) 10 hours.

- [13] J. Jin et al., “Volatile compound-mediated plant–plant interactions under stress with the tea plant as a model,” *Horticulture Research*, vol. 10, no. 9, p. uhad143, September 2023.
- [14] K. Matsui and J. Engelberth, “Green Leaf Volatiles—The Forefront of Plant Responses Against Biotic Attack,” *Plant and Cell Physiology*, vol. 63, no. 10, pp. 1378–1390, October 2022.
- [15] J. Engelberth, “Green Leaf Volatiles: A New Player in the Protection against Abiotic Stresses?” *International Journal of Molecular Sciences*, vol. 25, no. 17, p. 9471, January 2024.
- [16] T. Tanaka et al., “Identification of a Hexenal Reductase That Modulates the Composition of Green Leaf Volatiles,” *Plant Physiology*, vol. 178, no. 2, pp. 552–564, October 2018.
- [17] M. van Wijk, P. J. A. de Bruijn, and M. W. Sabelis, “Complex Odor from Plants under Attack: Herbivore’s Enemies React to the Whole, Not Its Parts,” *PLOS ONE*, vol. 6, no. 7, p. e21742, July 2011.
- [18] K. Sugimoto, K. Matsui, and J. Takabayashi, “Uptake and Conversion of Volatile Compounds in Plant–Plant Communication,” in *Deciphering Chemical Language of Plant Communication*, J. D. Blande and R. Glinwood, Eds. Cham: Springer International Publishing, 2016, pp. 305–316.
- [19] V. Jamali, A. Ahmadzadeh, W. Wicke, A. Noel, and R. Schober, “Channel Modeling for Diffusive Molecular Communication—A Tutorial Review,” *Proceedings of the IEEE*, vol. 107, no. 7, pp. 1256–1301, July 2019.
- [20] M. Yamane and A. Tani, “An absorption model of volatile organic compound by plant leaf: The most influential site in the absorption pathway,” *Atmospheric Environment: X*, vol. 23, p. 100274, August 2024.
- [21] N. M. Aguirre, J. M. Grunseich, A. F. Lima, S. D. Davis, and A. M. Helms, “Plant communication across different environmental contexts suggests a role for stomata in volatile perception,” *Plant, Cell & Environment*, vol. 46, no. 7, pp. 2017–2030, 2023.
- [22] K. Sugimoto et al., “Intake and transformation to a glycoside of (Z)-3-hexenol from infested neighbors reveals a mode of plant odor reception and defense,” *Proceedings of the National Academy of Sciences*, vol. 111, no. 19, pp. 7144–7149, May 2014.
- [23] Y. Aratani, T. Uemura, T. Hagihara, K. Matsui, and M. Toyota, “Green leaf volatile sensory calcium transduction in Arabidopsis,” *Nature Communications*, vol. 14, no. 1, p. 6236, October 2023.
- [24] M. Ameye et al., “Metabolomics Reveal Induction of ROS Production and Glycosylation Events in Wheat Upon Exposure to the Green Leaf Volatile Z-3-Hexenyl Acetate,” *Frontiers in Plant Science*, vol. 11, December 2020.
- [25] K. Sarang, K. J. Rudziński, and R. Szmigielski, “Green leaf volatiles in the atmosphere—properties, transformation, and significance,” *Atmosphere*, vol. 12, no. 12, 2021. [Online]. Available: <https://www.mdpi.com/2073-4433/12/12/1655>
- [26] F. Merdan and O. B. Akan, “Airborne particle communication through time-varying diffusion-advection channels,” 2026. [Online]. Available: <https://arxiv.org/abs/2601.08534>
- [27] B. E. Poling, J. M. Prausnitz, and J. P. O’Connell, *The Properties of Gases and Liquids*, 5th ed. New York: McGraw-Hill, 2001.
- [28] D. J. Warne, R. E. Baker, and M. J. Simpson, “Simulation and inference algorithms for stochastic biochemical reaction networks: From basic concepts to state-of-the-art,” *Journal of The Royal Society Interface*, vol. 16, no. 151, p. 20180943, February 2019.
- [29] P.-A. Lin et al., “Silencing the alarm: An insect salivary enzyme closes plant stomata and inhibits volatile release,” *New Phytologist*, vol. 230, no. 2, pp. 793–803, 2021.
- [30] R. Ospina and F. Marmolejo-Ramos, “Performance of Some Estimators of Relative Variability,” *Frontiers in Applied Mathematics and Statistics*, vol. 5, August 2019.
- [31] Chemo Database. cis-3-hexenal. Accessed: Sept. 21, 2025. [Online]. Available: <https://www.chemo.com/cid/46-326-9/3-Hexenal-Z>
- [32] —. cis-3-hexen-1-ol. Accessed: Sept. 21, 2025. [Online]. Available: <https://www.chemo.com/cid/18-655-5/3-Hexen-1-ol-Z>
- [33] —. cis-3-hexenyl acetate. Accessed: Sept. 21, 2025. [Online]. Available: <https://www.chemo.com/cid/54-175-8/3-Hexen-1-ol-acetate-Z>
- [34] U.S. Environmental Protection Agency. Indoor air unit conversions. Accessed: Sept. 21, 2025. [Online]. Available: <https://www3.epa.gov/ceampubl/learn2model/part-two/onsite/doc/Indoor%20Air%20Unit%20Conversions.pdf>
- [35] J. H. Seinfeld and S. N. Pandis, *Atmospheric Chemistry and Physics: From Air Pollution to Climate Change*, 2nd ed. New York: J. Wiley & sons, 2006.
- [36] D. Tolleter et al., “The Arabidopsis leaf quantitative atlas: A cellular and subcellular mapping through unified data integration,” *Quantitative Plant Biology*, vol. 5, p. e2, February 2024.

- [37] M. Durand, B. Porcheron, N. Hennion, L. Maurousset, R. Lemoine, and N. Pourtau, "Water Deficit Enhances C Export to the Roots in Arabidopsis thaliana Plants with Contribution of Sucrose Transporters in Both Shoot and Roots1[OPEN]," *Plant Physiology*, vol. 170, no. 3, pp. 1460–1479, March 2016.
- [38] I. H. Segel, *Enzyme Kinetics: Behavior and Analysis of Rapid Equilibrium and Steady-State Enzyme Systems*. New York: Wiley, 1975.
- [39] T. M. Cofer and J. H. Tumlinson, "The carboxylesterase AtCXE12 converts volatile (Z)-3-hexenyl acetate to (Z)-3-hexenol in Arabidopsis leaves," *Plant Physiology*, vol. 197, no. 4, p. kiaf119, April 2025.
- [40] T. Jing et al., "Glucosylation of (Z)-3-hexenol informs intraspecies interactions in plants: A case study in *Camellia sinensis*," *Plant, Cell & Environment*, vol. 42, no. 4, pp. 1352–1367, 2019.
- [41] K. Sugimoto et al., "Identification of a tomato UDP-arabinosyltransferase for airborne volatile reception," *Nature Communications*, vol. 14, no. 1, p. 677, February 2023.
- [42] B. Dubreuil, O. Matalon, and E. D. Levy, "Protein Abundance Biases the Amino Acid Composition of Disordered Regions to Minimize Non-functional Interactions," *Journal of Molecular Biology*, vol. 431, no. 24, pp. 4978–4992, December 2019.
- [43] PaxDb Consortium. Paxdb: Protein abundance database. Accessed: Sept. 24, 2025. [Online]. Available: <https://pax-db.org>



Fatih Merdan completed his high school education at Kirikkale Science High School. He received his B.Sc. degree in Electrical and Electronics Engineering from Middle East Technical University. He is currently pursuing his M.Sc. degree in Electrical and Electronics Engineering under the supervision of Prof. Akan at Koç University, Istanbul, Turkey.



Ozgur B. Akan (Fellow, IEEE) received the PhD from the School of Electrical and Computer Engineering Georgia Institute of Technology Atlanta, in 2004. He is currently the Head of Internet of Everything (IoE) Group, with the Department of Engineering, University of Cambridge, UK and the Director of Centre for neXt-generation Communications (CXC), Koç University, Turkey. His research interests include wireless, nano, and molecular communications and Internet of Everything.